NASA TECHNICAL NOTE

NASA TN D-5871

c. 1

NASA TN D-5871

COMPUTER AND ENGINE PERFORMANCE STUDY OF A GENERALIZED PARAMETER FUEL CONTROL FOR JET ENGINES

by Kurt Seldner and Harold Gold

Lewis Research Center
Cleveland, Ohio 44135

NATIONAL AERONAUTICS AND SPACE ADMINISTRATION • WASHINGTON, D. C. • JUNE 1970

1. Report No. NASA TN D-5871	2. Government Accession No.	3. Recipient's Catalog No.
4. Title and Subtitle COMPUTER AND ENGINE PERFORMANCE STUDY OF A GENERALIZED PARAMETER FUEL CONTROL FOR JET ENGINES		5. Report Date June 1970 6. Performing Organization Code
7. Author(s) Kurt Seldner and Harold Gold		8. Performing Organization Report No. E-5263
9. Performing Organization Name and Address Lewis Research Center National Aeronautics and Space Administration Cleveland, Ohio 44135		10. Work Unit No. 720-03 11. Contract or Grant No. 13. Type of Report and Period Covered Technical Note
12. Sponsoring Agency Name and Address National Aeronautics and Space Administration Washington, D.C. 20546		14. Sponsoring Agency Code

15. Supplementary Notes

16. Abstract

A mathematical analysis of a generalized parameter hydraulic fuel control concept is presented. An analog computer simulation was used to establish the feasibility of the fuel-control concept for jet engine applications. The simulation of the fuel control was first operated with a simulation of the J85-13 engine and then operated as an experimental control with an actual J85-13 engine in a test cell. Results obtained from the use of the simulated fuel control with both the simulated and actual engines are presented. The operation of the control is discussed, and its performance is compared with that of the normal J85-13 control.

17. Key Words *(Suggested by Author(s))* Aircraft Computers Propulsion systems	18. Distribution Statement Unclassified - unlimited

19. Security Classif. (of this report)	20. Security Classif. (of this page)	21. No. of Pages	22. Price*
Unclassified	Unclassified	39	$3.00

*For sale by the Clearinghouse for Federal Scientific and Technical Information Springfield, Virginia 22151

COMPUTER AND ENGINE PERFORMANCE STUDY OF A GENERALIZED PARAMETER FUEL CONTROL FOR JET ENGINES

by Kurt Seldner and Harold Gold

Lewis Research Center

SUMMARY

A mathematical analysis of a generalized parameter hydraulic fuel-control concept is presented. An analog computer simulation was used to establish the feasibility of the fuel-control concept for turbojet engine applications. The simulation of the fuel control was first operated with a simulation of the J85-13 engine and then operated as an experimental control with an actual J85-13 engine in a test cell. Results obtained from the use of the simulated fuel control with both the simulated and actual engines are presented. The operation of the control is discussed, and its performance is compared with that of the normal J85-13 control.

INTRODUCTION

An analysis of a fuel-control concept for turbojet engines is presented in this report. The analysis results from a study conducted at Lewis as a portion of a program to investigate engineering problems that affect production costs of turbojet engines. The objective of the cost study is to establish and demonstrate methods by which cost reductions may be achieved. Such reductions could significantly broaden the market for turbojet engines in general aviation. For these applications a control must be fully automatic and include all of the basic control functions. These include automatic engine startup, governing with maximum speed limiting, acceleration limiting, and deceleration limiting. A discussion of these factors is presented in references 1 and 2.

To satisfy the goal of low-cost, fuel-control system hardware should be less complex than that heretofore required for more conventional systems. Complex cams, transducers, and servosystems should be avoided. The fuel-control concept which has evolved in the study can be mechanized to meet this criterion. The concept is based on the approximation of engine acceleration and deceleration limits with functions based on cor-

rected parameters. The corrected parameter schedules are mechanized with hydraulic circuitry to form the control.

At the time of the evaluation of the fuel-control concept, both an analog simulation of the J85-13 engine and an actual J85-13 engine were available for the program. The fuel-control evaluation was thus performed with the J85-13 simulation and engine. Although this engine is equipped with an afterburner, it is otherwise similar to the engine types considered in low-cost applications. During the test program, the afterburner was not used, and the compressor variable geometry and the variable exhaust nozzle were programmed with their normal operating schedules.

The initial evaluation study was performed on an analog computer with a simulation of the J85-13 engine. The evaluation was then performed with a simulated fuel-control in combination with an electrohydraulic flow control and an actual J85-13 engine.

CONTROL PRINCIPLES

The fuel-control concept is based on the assumption that the maximum and minimum fuel limits can be described by linear functions of corrected engine parameters. A corrected parameter map illustrating these functions is presented in figure 1. The acceleration limit is defined by the relation

$$\frac{\dot{W}_T}{\delta\sqrt{\theta}} = \frac{N}{\sqrt{\theta}}\left(C_{11}\frac{P_3}{P_2} + C_{12}\right) \tag{1}$$

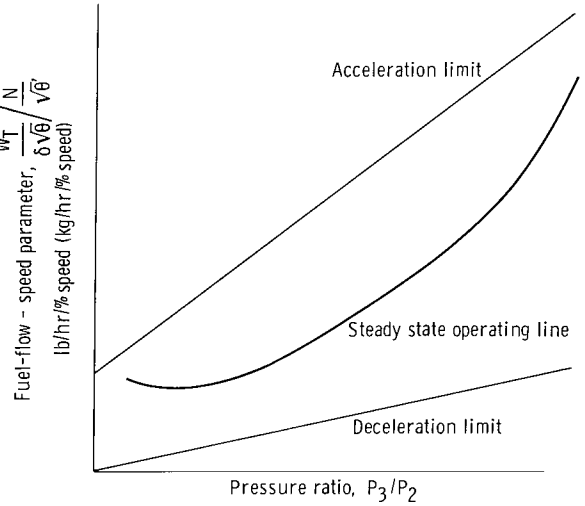

Figure 1. - Corrected parameter map employed in experimental fuel control.

and the deceleration limit by the relation

$$\frac{\dot{W}_T}{\delta\sqrt{\theta}} = \frac{N}{\sqrt{\theta}}\left(C_{10}\frac{P_3}{P_2}\right) \tag{2}$$

(Symbols are defined in appendix A.) These data were derived from approximations of the engine manufacturer's characteristics. As is shown in figure 2, different accelera-

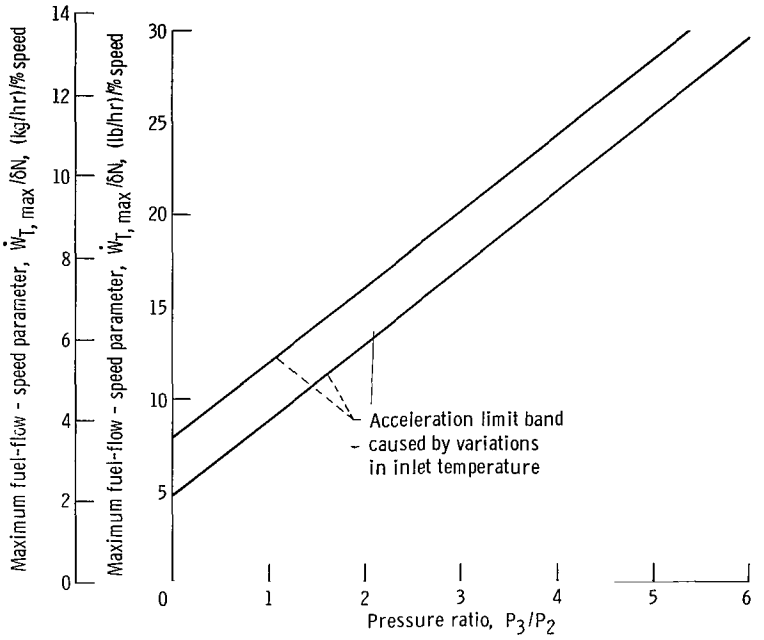

Figure 2. - Variation of J85-13 acceleration limits at different compressor inlet temperatures.

tion limits are required as the inlet temperature varies to prevent excessive turbine inlet temperatures. As can be seen from equation (1) the effects of inlet temperature are neglected in the control. The lower acceleration limit is thus used for all inlet temperatures. With this simplification, the maximum allowable fuel cannot be used for the lower temperature range. It is expected that the resulting lower acceleration capability is acceptable for general aircraft.

CONTROL MECHANIZATION

The hydraulic circuit employed in the fuel control is illustrated in figure 3. The cir-

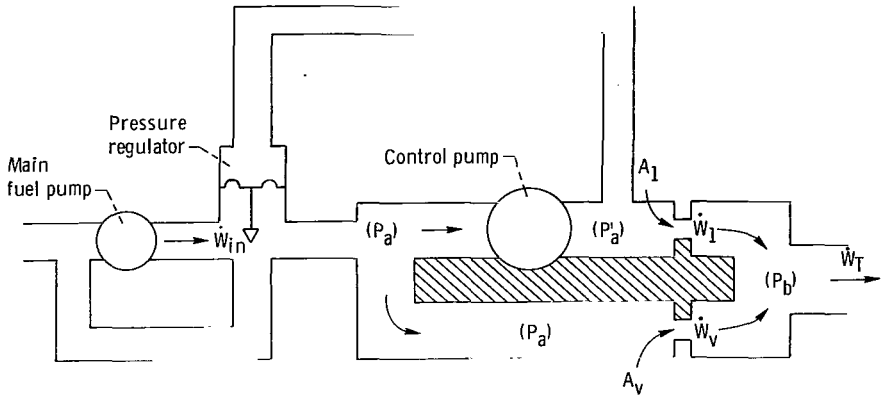

Figure 3. - Schematic drawing of basic hydraulic circuit used in experimental fuel control.

cuit generates an output flow rate $\dot{W}_T$ in accordance with the relation

$$\dot{W}_T = \frac{dN}{A_1}(A_1 + A_v) \tag{3}$$

The pressure regulator bypasses excess flow from the main fuel pump to regulate the pump discharge pressure P_a to the value of P'_a. Thus, the pressure difference across the control pump is zero, and the pressure differences across orifices A_1 and A_v are equal. These pressure relations yield the following expressions for fuel flow:

$$\dot{W}_1 = dN$$

and

$$\dot{W}_v = \frac{A_v}{A_1}\dot{W}_1$$

The total fuel flow is

$$\dot{W}_T = \dot{W}_1 + \dot{W}_v$$

Substituting the expressions for $\dot{W}_1$ and $\dot{W}_v$ yields equation (3).

It can be observed that the output flow (eq. (3)) is independent of discharge pressure P_b whenever the pressure regulator maintains a zero pressure drop across the control pump. In order to match the parameter map (see fig. 1) with the actual circuit (fig. 3), the bypass orifice A_v is composed of a series-parallel combination of orifices as shown in figure 4.

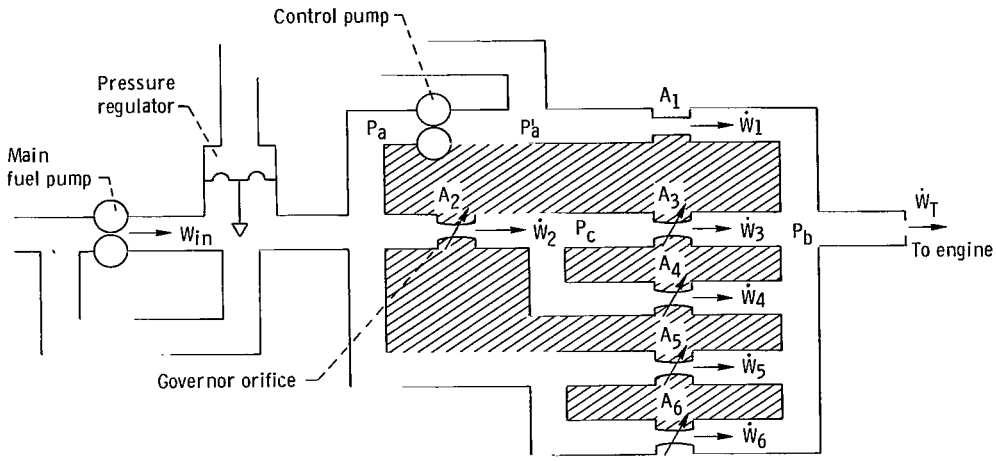

Figure 4. - Fuel-control system schematic.

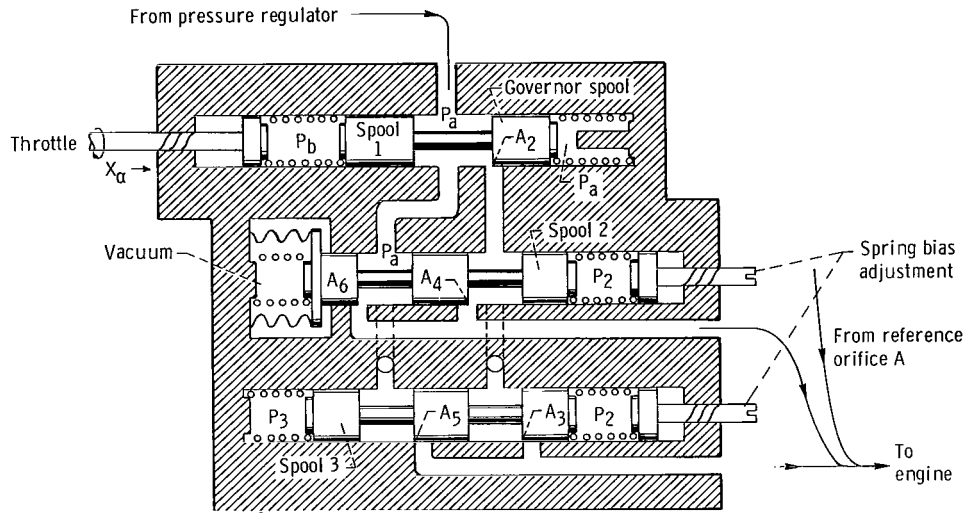

Figure 5. - Simplified cross section of fuel control valve.

A mechanical schematic of the fuel control variable orifice system is shown in figure 5. The areas of the various metering orifices are fixed by the spool positions which are, in turn, determined by the balance between the spring and pressure forces across the spool. The area of the governor orifices A_2 thus depends on the net force across the first spool. The forces acting on this piston consist of the differential pressure $(P_a - P_b)$ and the spring forces. The net forces applied are such that the governor area is closed at zero throttle position and a mechanical stop limits the maximum spool travel. The orifice areas A_4 and A_6 are fixed by the position of the second spool, which, in turn, is determined by the force balance between the compressor inlet pressure P_2 and

the spool return springs. The orifice areas A_3 and A_5 are similarly determined by a force balance between the pressure rise across the compressor and the spool return springs.

When the throttle is advanced, the force to the governor spool through the throttle spring is increased, thus advancing the governor spool until the force is balanced by the return spring and the differential pressure across the spool. For large throttle advances, the spool travel is limited by a mechanical stop. As engine speed increases, compressor discharge pressure P_3 also increases to advance the third spool. This spool opens orifice areas A_3 and A_5 to supply more fuel to the combustor. Concurrently, the differential pressure $(P_a - P_b)$ rises with speed thus applying a larger differential pressure across the orifice system and increasing the flow. The increase in $(P_a - P_b)$ also results in an increase in the return force on the governor spool and a corresponding reduction in A_2. An equilibrium condition is obtained whenever the power lever force applied to the springs is balanced by the force developed by the differential pressure $(P_a - P_b)$ at a constant or equilibrium speed.

ANALYSIS

Equations relating the fuel-control flow rate to throttle position and engine parameters such as speed, inlet pressure, and compressor pressure rise are developed in appendix B. It is shown in appendix B that the total flow to the engine is given by

$$\dot{W}_T = \frac{dN}{A_1}\left(A_1 + A_{C2} + \frac{A_{C1}A_2}{\sqrt{A_{C1}^2 + A_2^2}}\right) \tag{4}$$

The orifice area expressions are developed in appendix B as

$$A_{C1} = A_3 + A_4 = C_1 + C_2P_2 + C_3(P_3 - P_2) \tag{5}$$

$$A_{C2} = A_5 + A_6 = C_4 + C_5P_2 + C_6(P_3 - P_2) \tag{6}$$

The governor orifice area A_2 is a function of the spool position X_s

$$A_2 = f(X_s) \tag{7}$$

and the spool position X_s is a function of the throttle angle and engine speed

$$g(\alpha, N^2) = C_7\alpha - C_8N^2 - C_9 \tag{8}$$

$$\left.\begin{aligned} X_s &= g(\alpha, N^2) \qquad g \leq \overline{X}_s \\ X_s &= \overline{X}_s \qquad\quad g > \overline{X}_s \end{aligned}\right\} \tag{9}$$

Equations (4) to (9) define the behavior of the fuel control, relating the fuel-flow rate to engine speed, throttle position, and compressor inlet and discharge pressures. Because of the algebraic complexity of the set and the interaction of the control with the engine, the details of system operation will be discussed in conjunction with the system simulation.

The engine acceleration and deceleration limits, however, can be visualized directly from equation (4). During rapid accelerations, the governor orifice area A_2 becomes $\overline{A}_2$, where $\overline{A}_2$ is the full open governor orifice area. Therefore equation (4) becomes

$$\dot{W}_{T(max)} = \frac{dN}{A_1}\left(A_1 + A_{C2} + \frac{A_{C1}\overline{A}_2}{\sqrt{A_{C1}^2 + \overline{A}_2^2}}\right) \tag{10}$$

Because A_{C1} and A_{C2} are both functions of compressor inlet pressure and pressure rise, the acceleration limit is a function of speed, compressor inlet pressure, and compressor pressure rise.

During deceleration, the governor orifice closes and equation (4) becomes

$$\dot{W}_{T(min)} = \frac{dN}{A_1}(A_1 + A_{C2}) \tag{11}$$

The deceleration limit is thus a function of speed, compressor inlet pressure, and compressor pressure rise, as defined.

The analysis presented in appendix C relates the fuel-control design to engine fuel requirements. It is shown that the orifice areas A_{C1} and A_{C2} can be determined by considering expression (4) and the minimum and maximum engine fuel-flow requirements given by the linear relations

$$\frac{\frac{\dot{W}_T}{\delta\sqrt{\theta}}}{\frac{N}{\sqrt{\theta}}} = C_{10}\frac{P_3}{P_2} \qquad \text{(minimum flow)} \tag{12a}$$

$$\frac{\frac{\dot{W}_T}{\delta\sqrt{\theta}}}{\frac{N}{\sqrt{\theta}}} = C_{11}\frac{P_3}{P_2} + C_{12} \qquad \text{(maximum flow)} \tag{12b}$$

Equations (12) are rewritten in appendix C to yield expressions for uncorrected minimum and maximum fuel flow:

$$\left.\begin{aligned} \dot{W}_{T(min)} &= \frac{N}{P_r} C_{10}P_3 \\ \dot{W}_{T(max)} &= \frac{N}{P_r}\left[C_{10}P_3 + C_{12}P_2 + (C_{11} - C_{10})P_3\right] \end{aligned}\right\} \tag{13}$$

Comparing equations (13) with equations (10) and (11) and assuming that $\overline{A}_2^2 >> A_{C1}^2$ results in

$$\left.\begin{aligned} A_{C1} &= \frac{A_1}{P_{r_d}}\left[C_{12}P_2 + (C_{11} - C_{10})P_3\right] \\ A_{C2} &= \frac{A_1}{P_{r_d}} C_{10}P_3 - A_1 \end{aligned}\right\} \tag{14}$$

The equations for A_{C1} and A_{C2} are expressed in terms of compressor inlet and discharge pressures. The coefficients C_{10}, C_{11}, and C_{12} can be determined directly from the engine fuel limit requirements. The acceleration schedule is thus based on approximating the normal engine schedule to one based on equation (12b).

PROCEDURE

System Simulation

A nonlinear, high-frequency simulation of the J85-13 engine (ref. 3) was used. In

this simulation, each compressor stage is represented by its pressure and temperature maps. The momentum equation is used to establish the flow dynamics from the stage pressures. Energy and mass balance equations and an equation of state are used to compute the pressures and temperatures of each stage volume. Engine speed and compressor inlet pressure and temperature are input variables, thus allowing for variable operating conditions. An important feature of this dynamic model is that the compressor stall line is generated.

The basic energy, continuity, and momentum equations are used for the combustor and turbine simulation. The turbine pressure and enthalpy relations are obtained with two-dimensional maps. An enthalpy balance between the compressor and turbine is computed to obtain shaft torque, from which engine acceleration and speed are generated. The normal variable geometry schedules (inlet guide vanes, interstage bleed, and exhaust nozzle area) are included in the simulation.

Simulated Fuel Control and Engine

The fuel control was simulated on the analog computer and operated in conjunction with the J85-13 engine simulation. The information flow diagram of the control is pre-

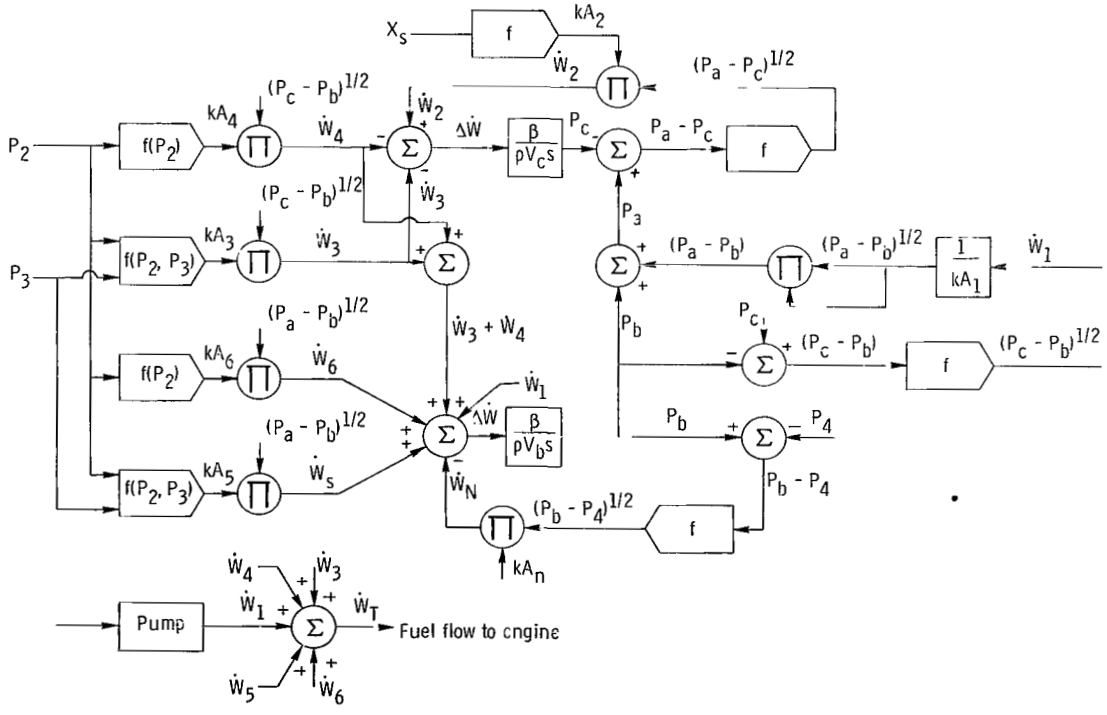

Figure 6. - Block diagram of fuel control.

sented in figure 6. The control simulation uses the basic component equations developed in appendix B with some modifications to avoid algebraic loops.

Standard orifice flow equations are used to compute the flow across the system orifices. The pressure in chamber C (see fig. 4) is computed from the relation

$$\dot{P}_c = \frac{\beta}{\rho V_c} (\dot{W}_2 - \dot{W}_3 - \dot{W}_4) \tag{15}$$

The pressure in the volume between the fuel-control burner spray nozzles is computed from the expression

$$\dot{P}_b = \frac{\beta}{\rho V_b} (\dot{W}_T - \dot{W}_N) \tag{16}$$

The flow areas A_3, A_4, A_5, and A_6 were simulated using equations (B18) to (B21). The equation for the governor spool position as a function of the spool forces is developed in appendix B as

$$(P_b - P_a)A_p - F_b + k_1(X_\alpha - X_s) - k_2 X_s = M\ddot{X}_s + D\dot{X}_s \tag{17}$$

Simulated Fuel Control with an Actual Engine

The fuel control was simulated on a small analog computer and used in combination with an electro-hydraulic flow regulator to control an actual J85-13 engine. The engine was equipped with the original fuel control, exhaust nozzle area, variable geometry, and interstage bleed controls. Provisions are included, however, to transfer control action to research fuel controls and to operate the controls off schedule.

The simulated fuel-control output signal was connected to a high-response electro-hydraulic flow regulator (ref. 4). Speed and pressure signals were fed back to the control from engine mounted transducers.

RESULTS AND DISCUSSION

Performance studies of the fuel control were conducted both open loop and with engine feedback. The objective of this effort was to establish the steady-state and dynamic performance of the fuel control.

The maximum and minimum values of fuel flow to speed parameter $\dot{W}_T/N\delta$ as a function of pressure ratio supplied by the control are presented in figure 7. These fuel-

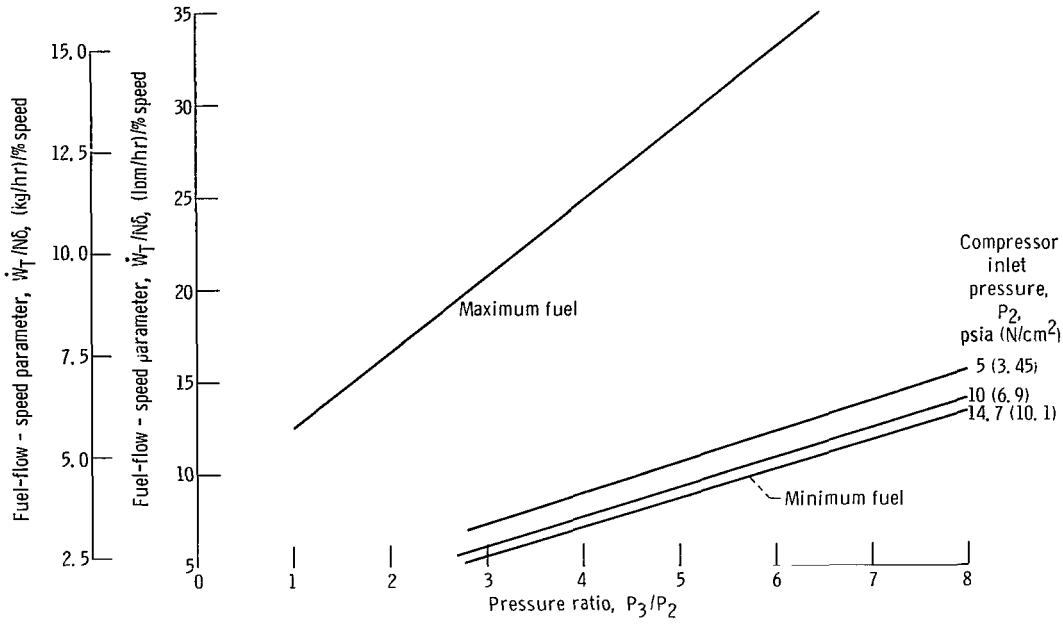

Figure 7. - Acceleration and deceleration limits for experimental fuel control.

flow limits correspond to equations (C17) and (C18) and approximately to equations (12a) and 12(b). As discussed in appendix C, the control mechanization is based on a design representing equations (C17) and (C18) and therefore includes a term inversely proportional to inlet pressure P_2. This term accounts for the spread observed for the minimum fuel flow limit in figure 7.

The J85-13 simulation was used to demonstrate the control concept and to observe the steady-state and dynamic performance. The parametric curves of $\dot{W}_T/N\delta$ as a function of pressure ratio and throttle position are presented for sea-level conditions in figure 8(a). Acceleration occurs along a line of constant throttle position (X_α line) to the final speed. It can be observed that at the extremes, the X_α lines converge to maximum and minimum limits. Similar curves for altitude conditions (25 000 ft (7600 m), M = 0.65) are presented in figure 8(b). It can be observed that the minimum $\dot{W}_T/N\delta$ limit varies as a function of inlet pressure P_2, as given by equation (C17). In addition, the X_α lines generated by the control are not identical to the sea-level condition.

Curves of fuel flow to pressure parameter $\dot{W}_T/P_3$ as a function of corrected engine speed and throttle position are shown for sea-level conditions in figure 9(a). With these coordinates, the slopes of the constant X_α lines between the maximum and minimum fuel limits are related to the gain of the proportional governor. As indicated by figure 9(a), in the vicinity of the acceleration limit, these lines are nearly horizontal because the governor is overridden by the acceleration limit. As the operating condition is ap-

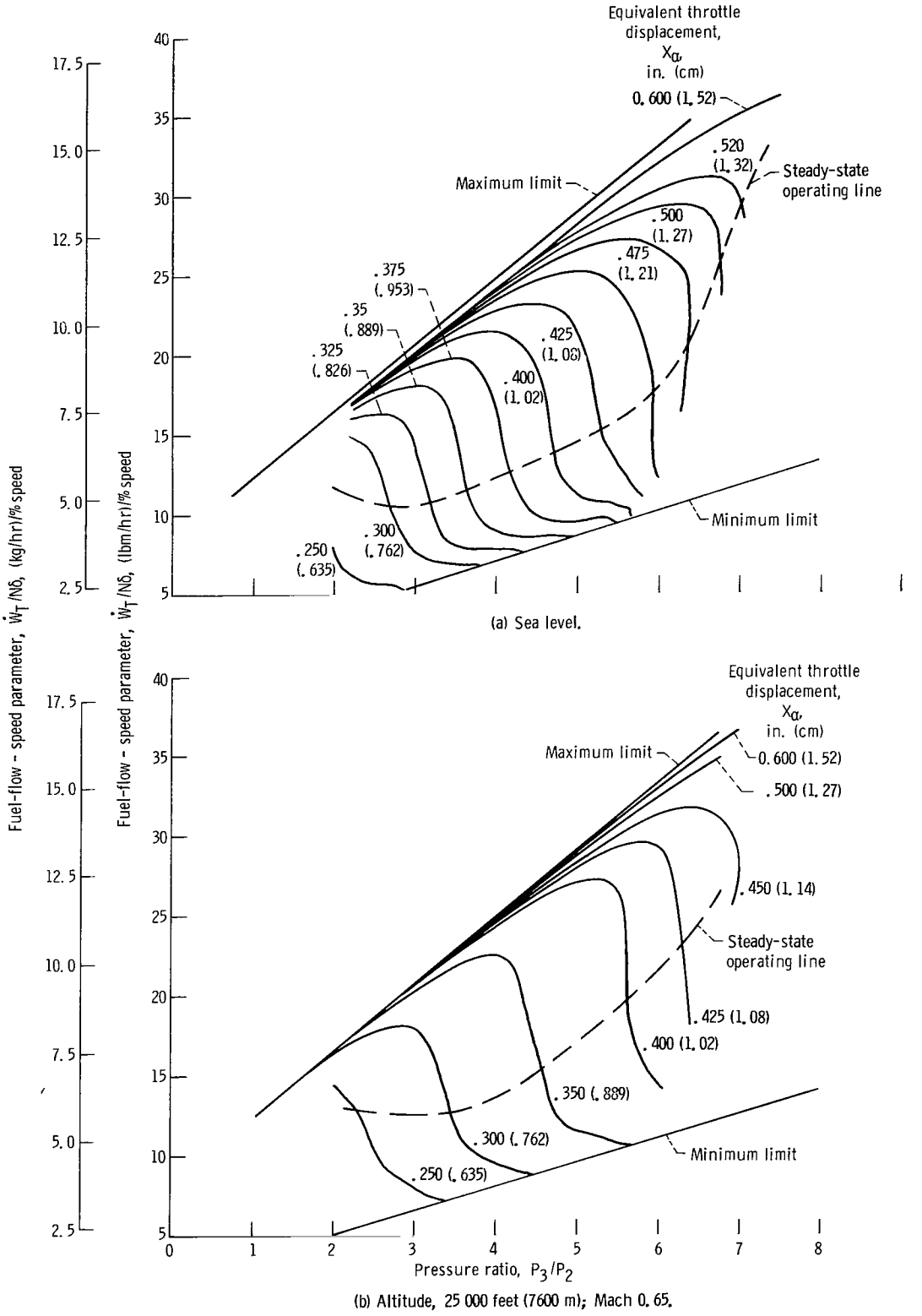

Figure 8. - Fuel-flow - speed parameter as function of pressure ratio for simulated engine and fuel control.

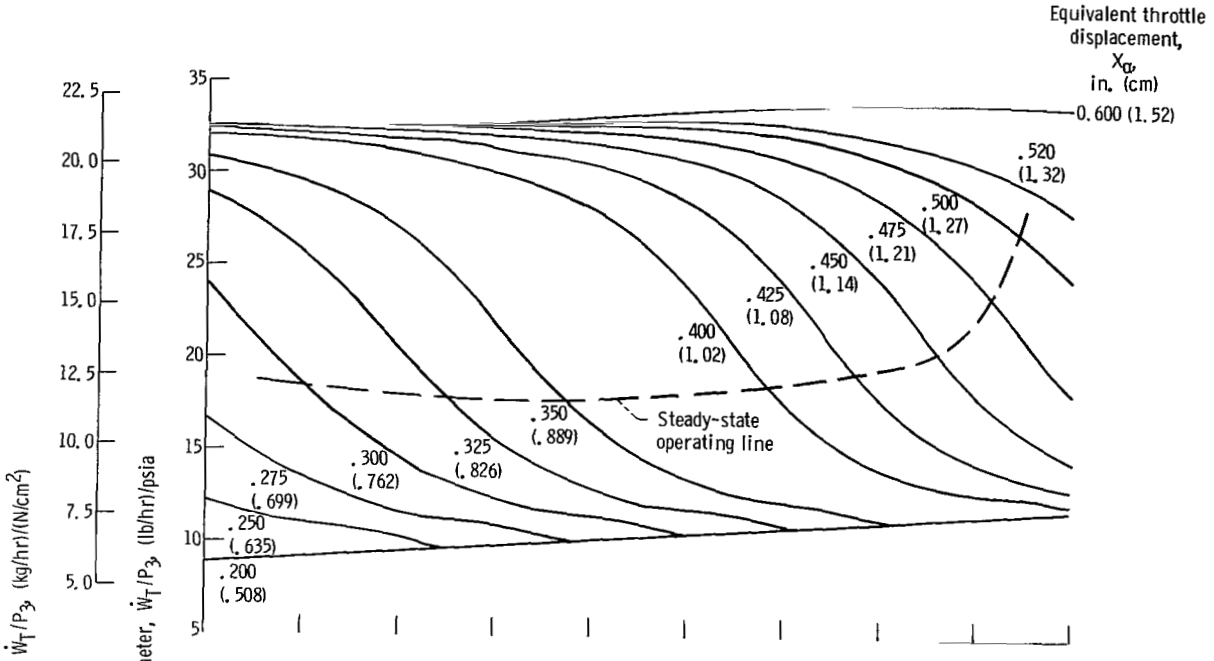

(a) Sea level.

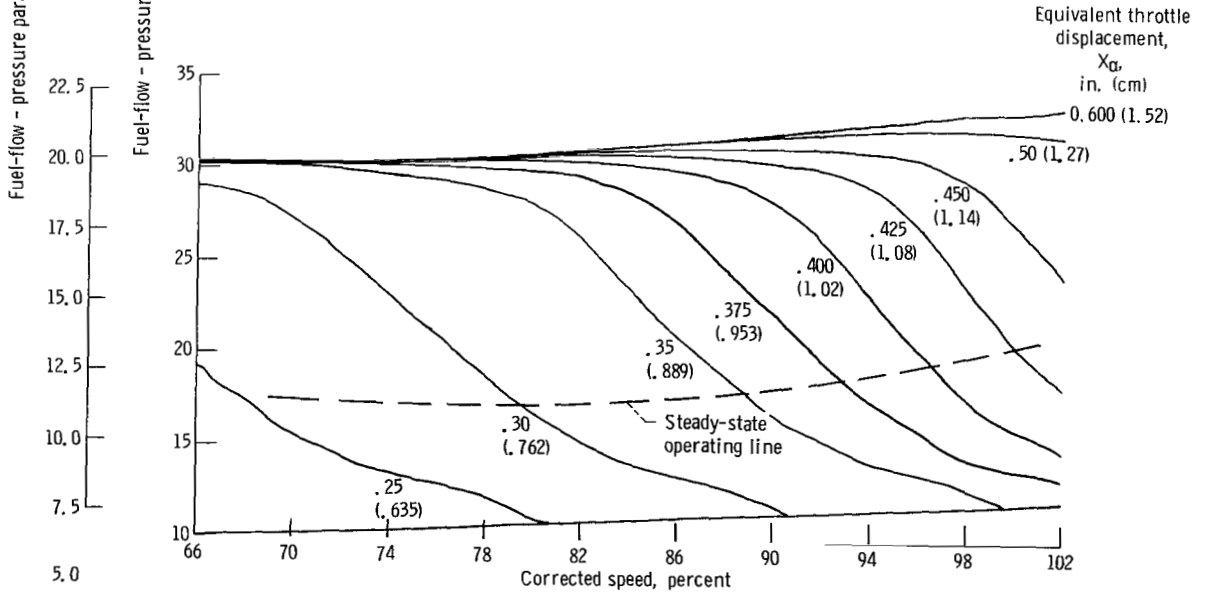

(b) Altitude, 25 000 feet (7600 m); Mach 0.65.

Figure 9. - Fuel-flow - pressure parameter as function of speed for simulated engine and fuel control.

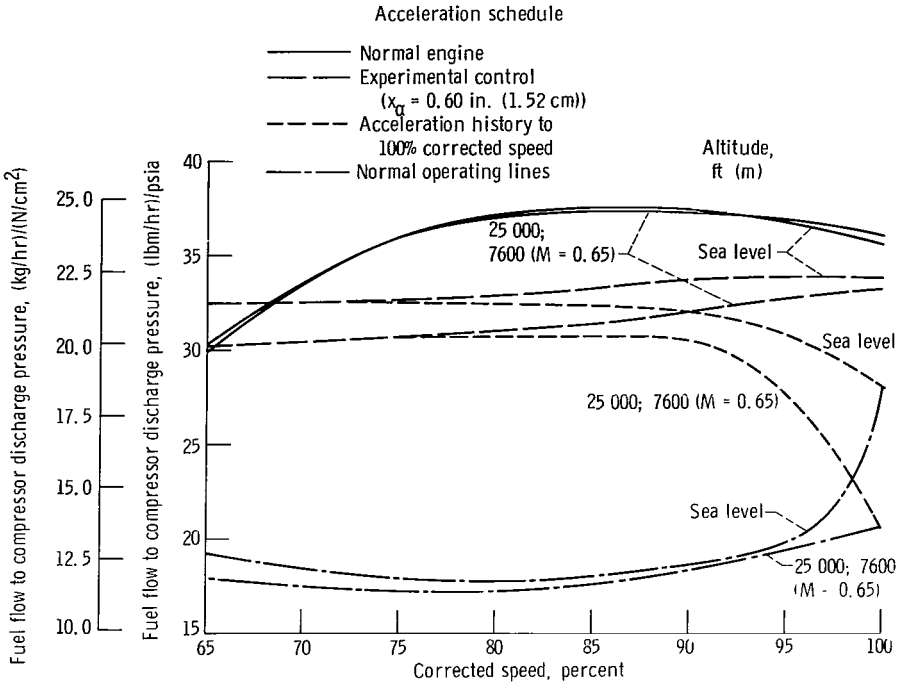

Figure 10. - Comparison of acceleration schedules

proached, governor action is restored, and the gain increases to provide good control performance. Similar curves for altitude condition are presented in figure 9(b).

Satisfactory fuel-control performance requires that the maximum fuel limit restrict engine operation to safe operating regions. Figure 10 presents the acceleration schedules for the experimental and engine manufacturer's controls. The engine steady-state operating lines are included to indicate the available acceleration margin. In addition, typical acceleration histories from near 70 to 100 percent corrected speed are shown for the experimental control. As the corrected speed begins to approach the 100-percent value, the trajectory leaves the acceleration schedule, and normal proportional control is restored. It can be seen from the tabulations of representative response times shown in table I, that for sea-level conditions the experimental and normal engine controls have equivalent response times. The experimental control regulates within the boundaries of the engine manufacturer's control except for a small excursion near idle speed.

The variation of mechanical engine speed as a function of equivalent throttle displacement X_α in steady state is presented in figure 11 for sea-level and altitude conditions. If the altitude dependency noted here is undesirable, inlet pressure or temperature corrections may be included in the design. The indicated values give the actual linear displacement of the governor spring and must be converted through a cam. It can be concluded from these curves that a physical limit must be designed into the power lever so that the engine design speed will not be exceeded. As an alternate approach, an altitude compensated throttle can be designed for the control.

TABLE I. - SUMMARY OF ENGINE RESPONSE TIME

[Sea level static.]

Speed, percent	Response time, sec		
	J85-13 engine with normal control	J85-13 engine with simulated experimental control	Simulated engine with simulated experimental control
70 - 100	0.71	0.7	0.80
80 - 90	.5	.3	.34
80 - 95	.5	.45	.47
80 - 100	[a].5	.5	.48
90 - 100	[a].3	----	.30

[a]Initial time to desired value additional settling time about 1.5 sec.

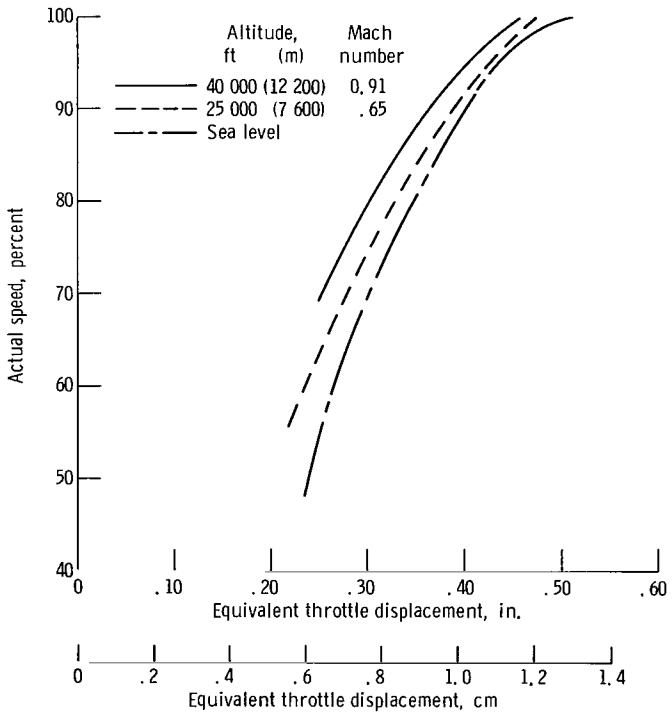

Figure 11. - Equivalent throttle displacement as function of actual speed.

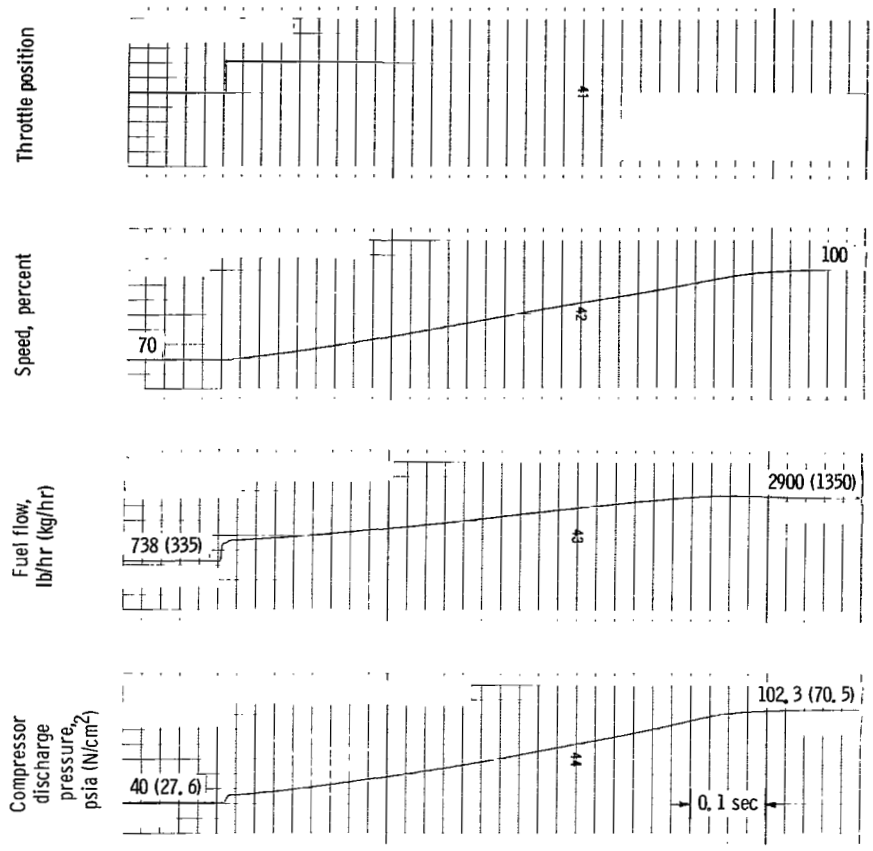

(a) Acceleration, 70 to 100 percent speed.

Figure 12. - Dynamic response of simulated engine to throttle command (sea level) for engine acceleration of 70 to 100 percent.

The J85-13 engine and fuel-control simulations were also subjected to throttle disturbances to determine the acceleration and deceleration characteristics at sea level and at 40 000 feet (12 200 m) altitude (M = 0.91). Figure 12(a) presents a recording of the engine acceleration from 70 to 100 percent speed. For this throttle advance, the governor area was forced fully open and the engine accelerated to the desired operating speed in about 0.8 second. Engine acceleration response from 90 to 100 percent is illustrated in figure 12(b). For this case, the magnitude of the disturbance was insufficient to force the governor area to the fully open position. The response time for the 90 to 100 percent speed change was 0.3 second.

Engine deceleration from 100 to 70 percent is illustrated in figure 13. This throttle chop caused the governor orifice to close. The time required to decrease the speed to the desired condition is about 1.6 seconds.

The system performance was also evaluated at 40 000 feet (12 200 m) and Mach 0.91. A representative recording illustrating acceleration from 90 to 100 percent speed is pre-

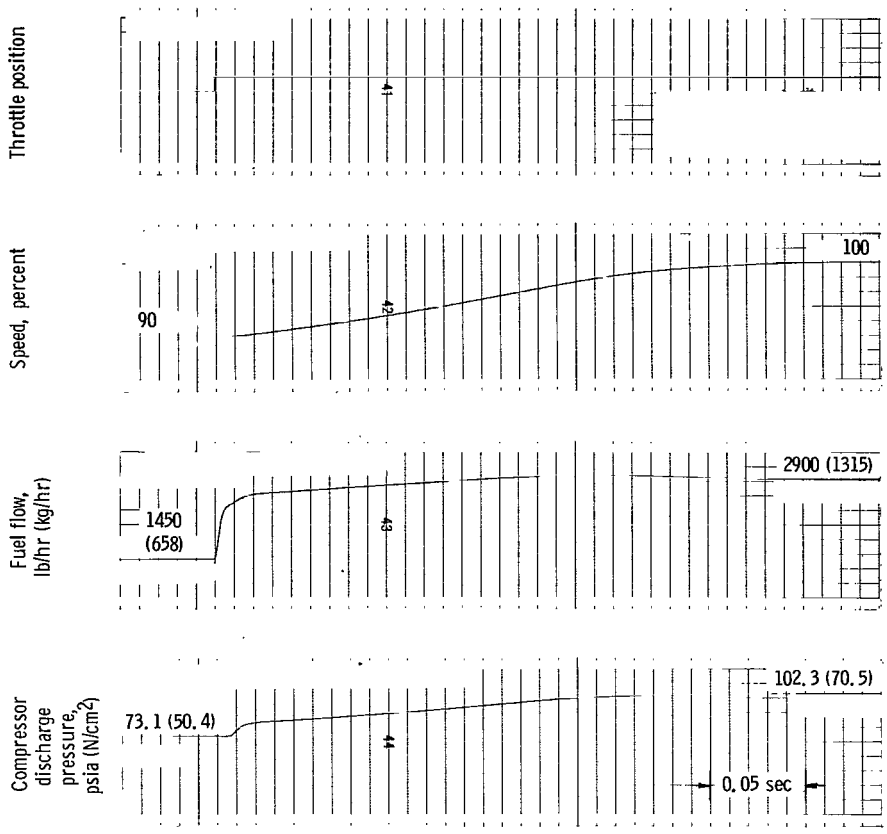

(b) Acceleration, 90 to 100 percent speed.

Figure 12. - Concluded.

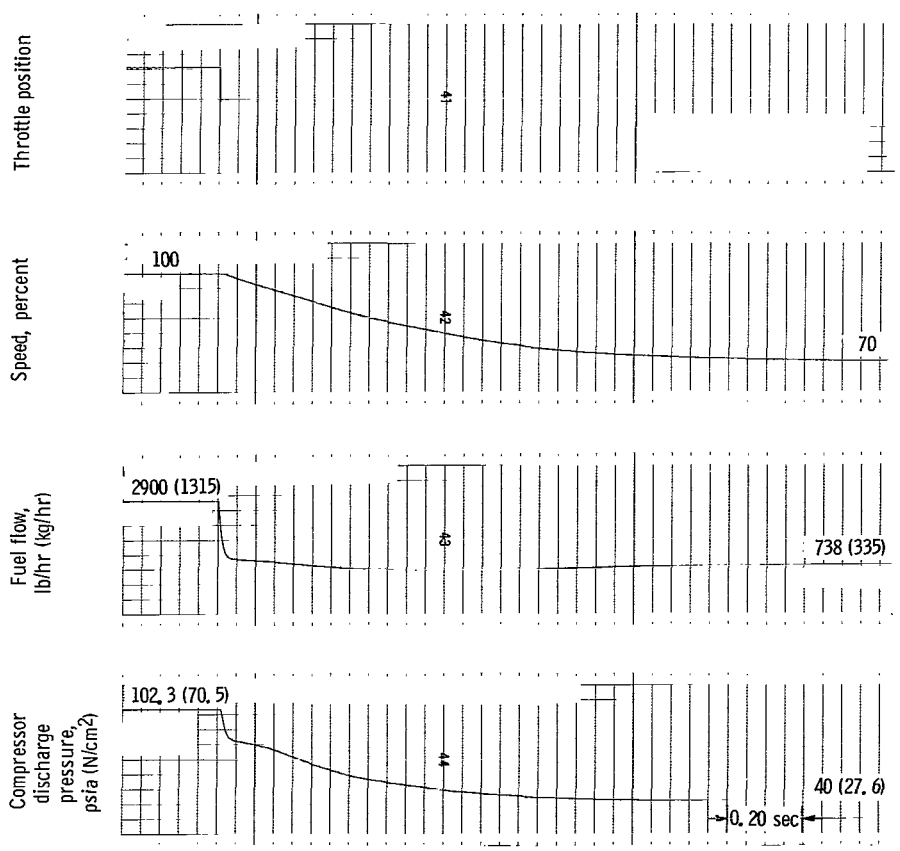

Figure 13. - Dynamic response of simulated engine to throttle chop at sea level. Engine deceleration, 100 to 70 percent speed.

sented in figure 14. The time required to achieve the steady-state condition is about 3.0 seconds. A similar response for engine deceleration is shown in figure 15. The results indicate that a 100 to 90 percent speed change was accomplished within 3.0 seconds.

The response of the actual J85-13 engine with the simulated control is shown in figure 16. These tests demonstrated the effectiveness of the acceleration limit in preventing engine stall at sea-level conditions. A typical response from 70 to 99 percent speed is illustrated in figure 16(a). This speed change was accomplished within 0.7 second. A similar recording showing a 90 to 99 percent speed change is presented in figure 16(b). This step change was achieved within 0.3 second. During the test program with the actual J85-13 engine, step commands were restricted to 99 percent

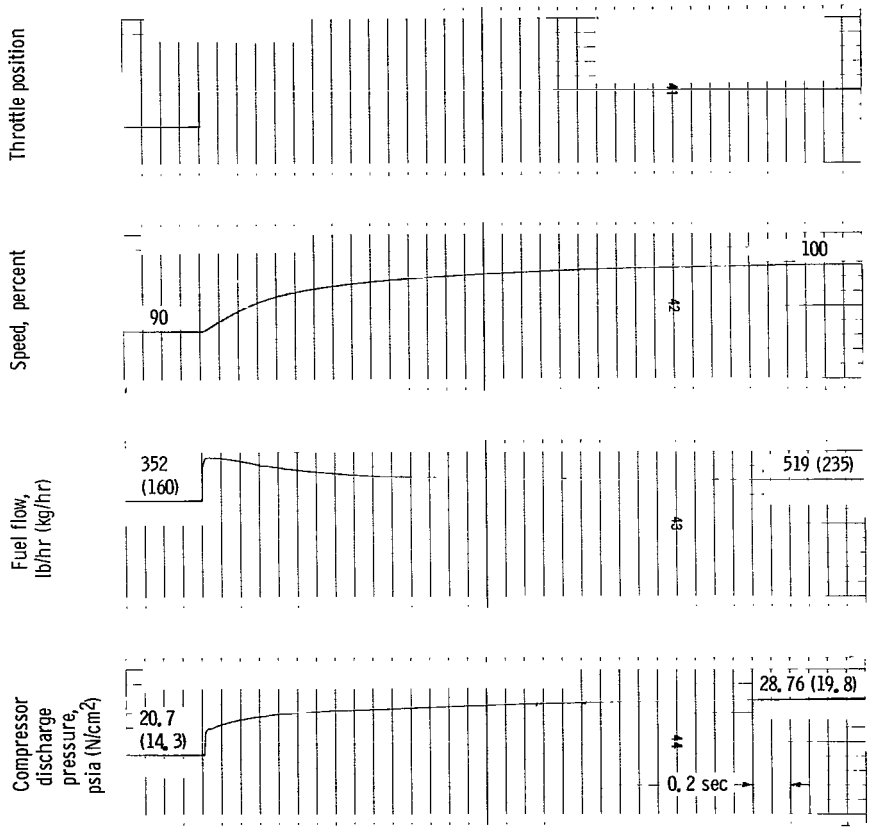

Figure 14. - Dynamic response simulated engine to throttle command at 40 000 feet (12 200 m) and Mach 0.91. Engine acceleration, 90 to 100 percent speed.

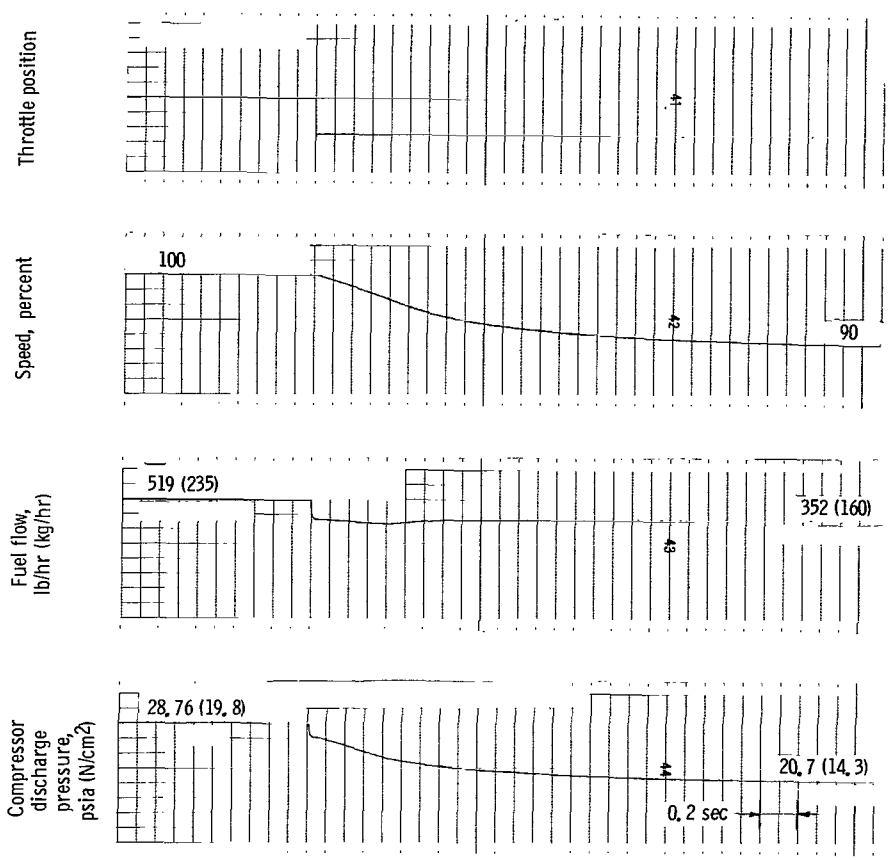

Figure 15. - Dynamic response of simulated engine to throttle chop at 40 000 feet (12 200 m) and Mach 0.91. Engine deceleration, 100 to 90 percent speed.

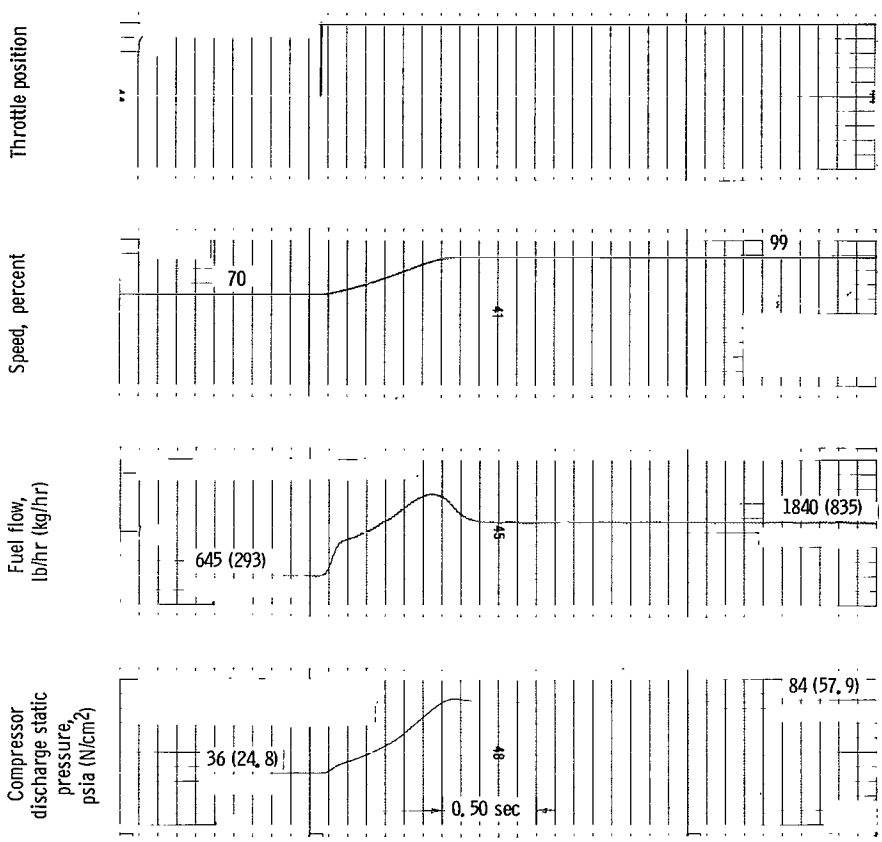

(a) Acceleration, 70 to 99 percent speed.

Figure 16. - Dynamic response of actual engine to throttle command at sea level.

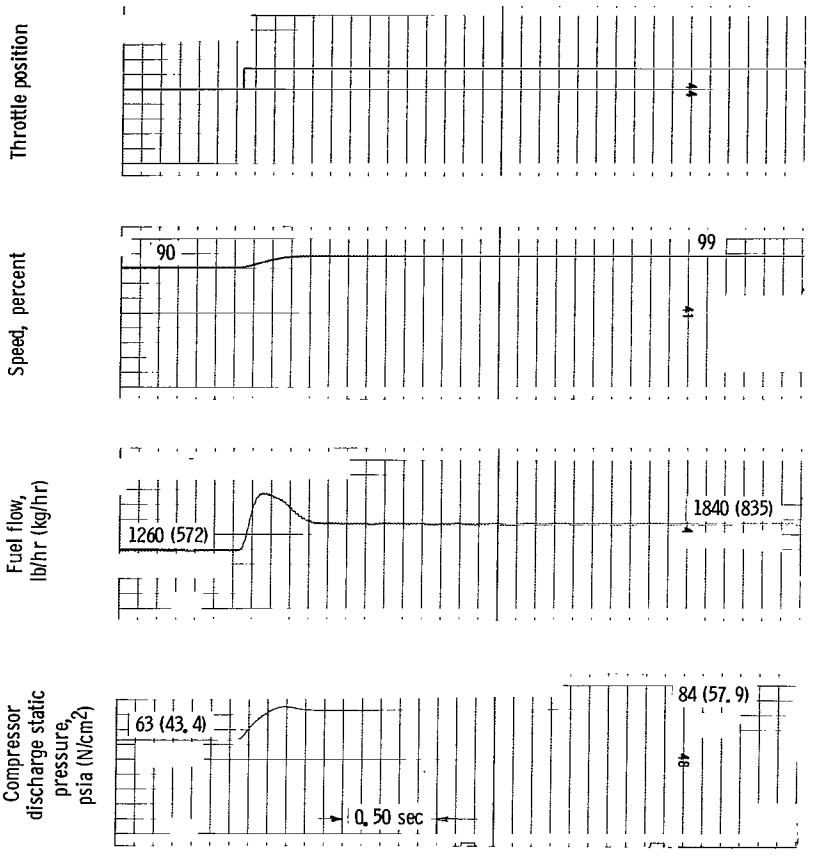

(b) Acceleration, 90 to 99 percent speed.

Figure 16. - Concluded.

maximum speed or less. The restriction was imposed to eliminate any possibility of afterburner light-off.

During engine acceleration, the exhaust nozzle was incorrectly scheduled. This schedule resulted in lower steady-state fuel flow. For this reason, the results obtained from the engine simulation at sea level (fig. 12) do not fully correspond to the actual engine tests (fig. 16). The exhaust nozzle area variation of the simulated engine was matched to that of the test engine. The performance for a 70 to 99 percent speed dis-

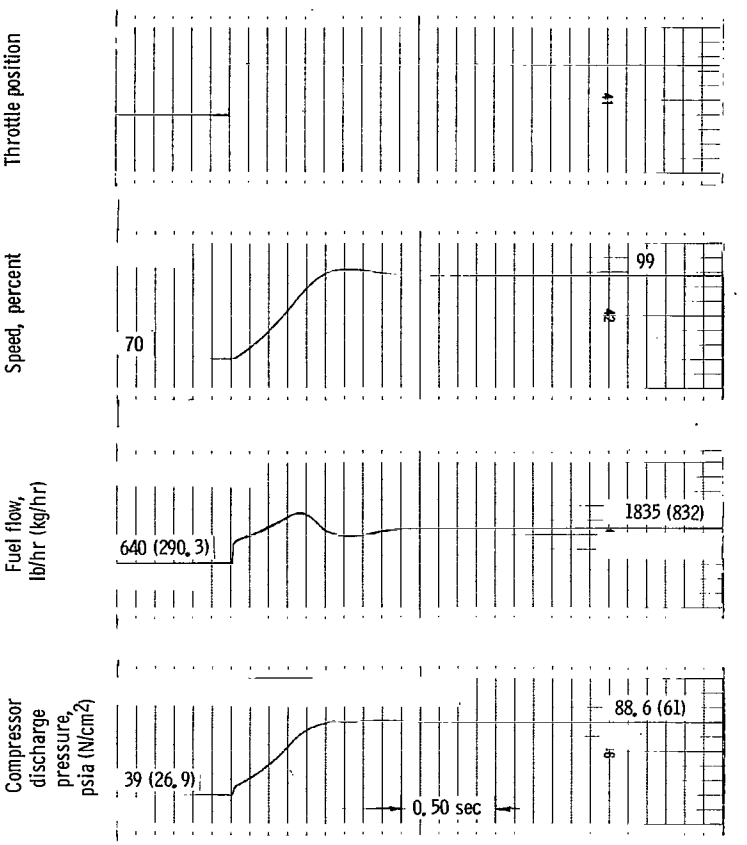

Figure 17. - Dynamic response of simulated engine with off-schedule exhaust nozzle area at sea level. Engine acceleration, 70 to 99 percent speed.

turbance is shown in figure 17. A settling time of 0.8 second was obtained. The 2-percent speed overshoot can be attributed to the difference in exhaust nozzle movement. A similar recording for a 90 to 99 percent speed change is presented in figure 18. This step change was accomplished within 0.4 second. A tabulation of representative system response times is presented in table I. The tabulation includes response times obtained from the actual engine and its normal controls, the actual engine with the simulated experimental control, and the engine simulation with the simulated control. The data presented indicate that the performance obtained from the control concept examined in this report compares favorably to that obtained with the original engine controls.

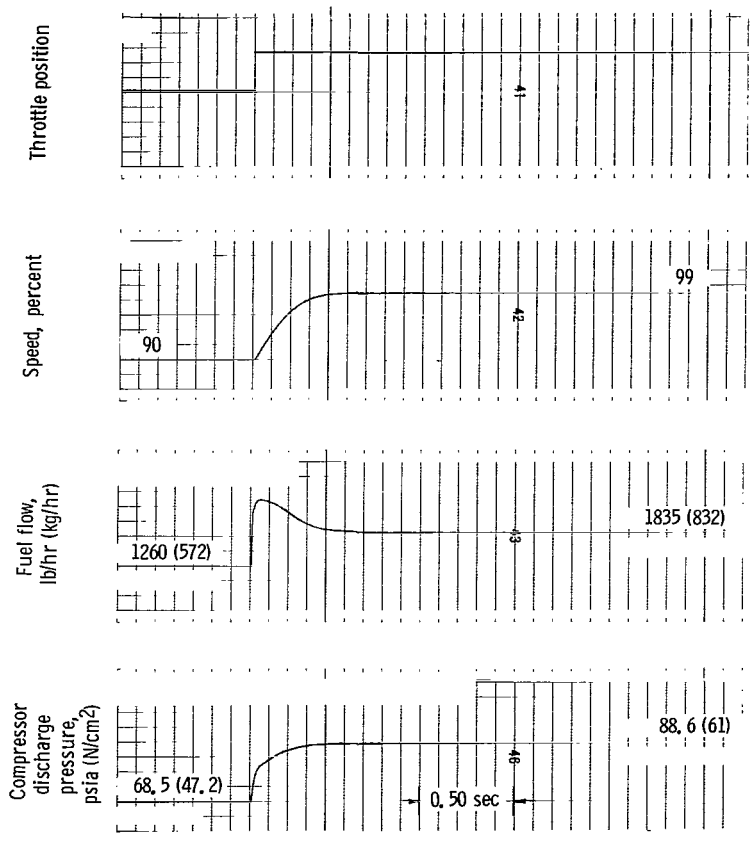

Figure 18. - Dynamic response of simulated engine with off-schedule exhaust nozzle area at sea level. Engine acceleration, 90 to 99 percent speed.

CONCLUSIONS

The fuel-control tests with the actual J85-13 engine indicate that satisfactory steady-state and dynamic performance can be achieved. The acceleration limiter was effective in preventing engine stall.

The tests conducted with the simulated J85-13 engine at sea-level and altitude conditions indicate satisfactory performance over the desired operating range. The control effectively restricted engine operation within permissible limits.

The results of the analytical and test programs indicate that the techniques employed in the design of the generalized parameter hydraulic fuel control are satisfactory for single-spool turbojet engines. The original objectives of the control design were met, and the results show that the inherent simplifications do not affect the dynamic performance of the control-engine system.

Lewis Research Center,
National Aeronautics and Space Administration,
Cleveland, Ohio, November 4, 1969,
720-03.

APPENDIX A

SYMBOLS

A_{C1} sum of orifice areas A_3 and A_4, $in.^2$; cm^2

A_{C2} sum of orifice areas A_5 and A_6, $in.^2$; cm^2

A_i general orifice area, $in.^2$; cm^2

A_N spray bar nozzle area, $in.^2$; cm^2

A_p governor piston area, $in.^2$; cm^2

A_v bypass orifice area, $in.^2$; cm^2

A_1 reference orifice area, $in.^2$; cm^2

A_2 governor area, $in.^2$; cm^2

$\overline{A}_2$ maximum governor area, $in.^2$; cm^2

A_3 orifice area, $f(P_3, P_2)$, $in.^2$; cm^2

A_4 orifice area, $f(P_2)$, $in.^2$; cm^2

A_5 orifice area, $f(P_3, P_2)$, $in.^2$; cm^2

A_6 orifice area, $f(P_2)$, $in.^2$; cm^2

a_{31} area coefficient

a_{32} area coefficient

a_{41} area coefficient

a_{42} area coefficient

a_{51} area coefficient

a_{52} area coefficient

a_{61} area coefficient

a_{62} area coefficient

C_i constants ($i = 1, \ldots, n$)

D damping coefficient, (lbf)(sec)/in.; (N)(sec)/m

d pump flow coefficient, (lb)(hr)/% speed; (kg)(hr)/% speed

F_b bias force, lbf; N

k	orifice flow conversion constant, lbm/(hr)(in.^{2}) (lbf/in.^{2})$^{1/2}$; kg/(hr)(cm^2) (N/cm^2)$^{1/2}$
k_1	spring constant, lbf/in.; N/cm
k_2	spring constant, lbf/in.; N/cm
M	mass of governor spool, lbm; kg
N	engine speed, percent of rated speed
P_a	pressure, lbf/in.^{2}; N/cm^2
P'_a	pressure, lbf/in.^{2}; N/cm^2
P_b	pressure, lbf/in.^{2}; N/cm^2
$\dot{P}_b$	rate of change of pressure, (lbf)(in.^{2})/sec; N/cm^2/sec
P_c	pressure, lbf/in.^{2}; N/cm^2
$\dot{P}_c$	rate of change of pressure, (lbf/in.^{2})/sec; (N/cm^2)/sec
ΔPi	general differential pressure, lbf/in.^{2}; N/cm^2
P_r	reference pressure, lbf/in.^{2}; N/cm^2
P_2	compressor inlet pressure, lbf/in.^{2}; N/cm^2
P_3	compressor discharge pressure, lbf/in.^{2}; N/cm^2
P_4	burner pressure, lbf/in.^{2}; N/cm^2
s	Laplace operator
T_2	inlet temperature, ^{o}R; K
t	time, sec
V_b	volume of chamber b, in.^{3}; cm^3
V_c	volume of chamber c, in.^{3}; cm^3
$\Delta\dot{W}_B$	net fuel flow, lbm/hr; kg/hr
$\Delta\dot{W}_C$	net fuel flow, lbm/hr; kg/hr
$\dot{W}_i$	general fuel flow, lbm/hr; kg/hr
$\dot{W}_N$	spray bar fuel flow, lbm/hr; kg/hr
$\dot{W}_T$	total fuel flow, lbm/hr; kg/hr
$\dot{W}_{T(max)}$	acceleration fuel flow, lbm/hr; kg/hr
$\dot{W}_{T(min)}$	deceleration fuel flow, lbm/hr; kg/hr
$\dot{W}_v$	bypass fuel flow, lbm/hr; kg/hr

$\dot{W}_1$ fuel flow through orifice A_1, lbm/hr; kg/hr

$\dot{W}_2$ fuel flow through orifice A_2, lbm/hr; kg/hr

$\dot{W}_3$ fuel flow through orifice A_3, lbm/hr; kg/hr

$\dot{W}_4$ fuel flow through orifice A_4, lbm/hr; kg/hr

$\dot{W}_5$ fuel flow through orifice A_5, lbm/hr; kg/hr

$\dot{W}_6$ fuel flow through orifice A_6, lbm/hr; kg/hr

X_α equivalent linear displacement of throttle, in.; cm

X_s linear displacement of governor spool, in.; cm

$\overline{X}_s$ maximum displacement of governor spool, in.; cm

α angular throttle motion, rad

$\Delta\alpha$ change of throttle motion, rad

β bulk modulus, lbf/in.^{2}; N/cm^2

δ $P_2/14.7$; $P_2/10.1$

$\sqrt{\theta}$ $\sqrt{T_2/518.7}$; $\sqrt{T_2/288}$

ρ fuel density, lbm/in.^{3}; kg/cm^3

APPENDIX B

SYSTEM EQUATIONS

The weight flow across the various orifices of the fuel control can be described by equations of the form

$$\dot{W}_i = kA_i \sqrt{\Delta P_i} \tag{B1}$$

where the density term is assumed constant and included in the coefficient k. For the six orifices of the system shown in the schematic of figure 1, this equation becomes

$$\dot{W}_1 = kA_1 \sqrt{P_a - P_b} \tag{B2}$$

$$\dot{W}_2 = kA_2 \sqrt{P_a - P_c} \tag{B3}$$

$$\dot{W}_3 = kA_3 \sqrt{P_c - P_b} \tag{B4}$$

$$\dot{W}_4 = kA_4 \sqrt{P_c - P_b} \tag{B5}$$

$$\dot{W}_5 = kA_5 \sqrt{P_a - P_b} \tag{B6}$$

$$\dot{W}_6 = kA_6 \sqrt{P_a - P_b} \tag{B7}$$

and the final fuel flow through the spray bar nozzle into the engine is

$$\dot{W}_N = kA_N \sqrt{P_b - P_4} \tag{B8}$$

Since the flow through the governor orifice A_2 passes through A_3 and A_4,

$$\dot{W}_2 = \dot{W}_3 + \dot{W}_4 \tag{B9}$$

Equations (B3) to (B5) can be combined with equation (B9) to give an expression for the intermediate pressure P_c:

$$P_c = \frac{A_2^2 P_a + (A_3 + A_4)^2 P_b}{(A_3 + A_4)^2 + A_2^2}$$

Defining $A_3 + A_4$ as A_{C1}

$$P_c = \frac{A_2^2 P_a + A_{C1}^2 P_b}{A_2^2 + A_{C1}^2} \tag{B10}$$

and

$$\dot{W}_3 + \dot{W}_4 = k\left(\frac{A_{C1}^2 A_2^2}{A_{C1}^2 + A_2^2}\right)^{1/2} (P_a - P_b)^{1/2} \tag{B11}$$

If the flows $\dot{W}_5$ and $\dot{W}_6$ are summed

$$\dot{W}_5 + \dot{W}_6 = kA_{C2}(P_a - P_b)^{1/2} \tag{B12}$$

where

$$A_{C2} = A_5 + A_6$$

The flow through the control pump is proportional to the engine speed, hence

$$\dot{W}_1 = dN \tag{B13}$$

Combining equations (B2) and (B13) yields

$$(P_a - P_b)^{1/2} = \frac{dN}{kA_1} \tag{B14}$$

Substituting the differential pressure from equation (B14) into equations (B11) and (B12) results in

$$\dot{W}_3 + \dot{W}_4 = \left(\frac{A_{C1}^2 A_2^2}{A_{C1}^2 + A_2^2}\right)^{1/2} \frac{dN}{A_1} \tag{B15}$$

$$\dot{W}_5 + \dot{W}_6 = A_{C2} \frac{dN}{A_1} \tag{B16}$$

The total fuel flow to the engine can now be computed from equations (B13), (B15), and (B16) as

$$\dot{W}_T = \frac{dN}{A_1}\left(A_1 + A_{C2} + \frac{A_{C1}A_2}{\sqrt{A_{C1}^2 + A_2^2}}\right) \tag{B17}$$

Equation (B17) relates the engine fuel flow, shaft speed, and the various area terms. The flow areas are determined as illustrated in figure 4, by the force balance between the pressure and spring forces applied across the spools of the fuel control.

The areas A_4 and A_6, which are determined by the position of the second spool, can thus be described by

$$A_4 = a_{41} + a_{42}P_2 \tag{B18}$$

$$A_6 = a_{61} + a_{62}P_2 \tag{B19}$$

Similarly, A_3 and A_5 are determined by the position of the third spool:

$$A_3 = a_{31} + a_{32}(P_3 - P_2) \tag{B20}$$

$$A_5 = a_{51} + a_{52}(P_3 - P_2) \tag{B21}$$

The combined area terms A_{C1} and A_{C2} of equation (B17) can be formed from equations (B18) to (B21), where

$$A_{C1} = A_3 + A_4 = C_1 + C_2P_2 + C_3(P_3 - P_2) \tag{B22}$$

$$A_{C2} = A_5 + A_6 = C_4 + C_5P_2 + C_6(P_3 - P_2) \tag{B23}$$

The coefficients C_i can be determined from the areas, spring constants, and flow area against stroke characteristic of the system. The area characteristics for the orifices controlled by the second and third spools are linear functions of spool position, but the governor orifice area is a nonlinear function of the stroke of its spool.

It can be seen from figure 5 that, as the throttle is advanced through an angle $\Delta\alpha$, the throttle cam converts the rotation to a linear advance against the throttle spring. The spring, in turn, raises the forces on the spool tending to increase the governor orifice area A_2. If the throttle advance $\Delta\alpha$ is sufficiently large, the spool motion is limited by a mechanical stop. The spool response to throttle position can be described by

$$(P_b - P_a)A_p - F_b + k_1(X_\alpha - X_s) - k_2X_s = M\ddot{X}_s + D\dot{X}_s \tag{B24}$$

Neglecting the dynamics of the mass spring system reduces equation (B24) to

$$(P_b - P_a)A_p - F_b + k_1(X_\alpha - X_s) - k_2X_s = 0 \tag{B25}$$

Since

$$(P_a - P_b) \propto N^2$$

The equation reduces to

$$-N^2A_b + k_1X_\alpha - (k_1 + k_2)X_s - F_b = 0 \tag{B26}$$

A nonlinear relation could exist between power lever and throttle spring position. However, for this analysis, this function was assumed to be linear. Equation (B26) becomes

$$\left.\begin{aligned} g(\alpha, N^2) &= C_7\alpha - C_8N^2 - C_9 \\ X_s &= g(\alpha, N^2) \qquad g \leq \overline{X}_s \\ X_s &= \overline{X}_s \qquad g > \overline{X}_s \end{aligned}\right\} \tag{B27}$$

The governor orifice area A_2 is a logarithmic function of the throttle position X_s:

$$A_2 = f(X_s) \tag{B28}$$

The nonlinear characteristic was selected to compensate for the higher ratio of engine speed to fuel gain encountered for the lower speed region. By this method the overall system gain can be modified to prevent instability.

APPENDIX C

FUEL CONTROL ORIFICE SIZING

Once the basic design of the fuel control is established, the control components must be sized to satisfy the fuel requirements of the engine. An expression for the total flow from the control to the engine was developed in appendix B as

$$\dot{W}_T = \frac{Nd}{A_1}\left(A_1 + A_{C2} + \frac{A_{C1}A_2}{\sqrt{A_{C1}^2 + A_2^2}}\right) \tag{C1}$$

For minimum flow the governor area A_2 is fully closed and expression (C1) reduces to

$$\dot{W}_{T(min)} = \frac{Nd}{A_1}(A_1 + A_{C2}) \tag{C2}$$

Similarly, for maximum flow the governor area A_2 is fully open and equation (C1) becomes

$$\dot{W}_{T(max)} = \frac{Nd}{A_1}\left(A_1 + A_{C2} + \frac{A_{C1}\bar{A}_2}{\sqrt{A_{C1}^2 + \bar{A}_2^2}}\right) \tag{C3}$$

where $\bar{A}_2 = A_{2max}$

Assuming that $\bar{A}_2^2 >> A_{C1}^2$, equation (C3) reduces to

$$\dot{W}_{T(max)} \cong \frac{Nd}{A_1}(A_1 + A_{C2} + A_{C1}) \tag{C4}$$

The fuel-control concept is based on the assumption that the minimum and maximum fuel-flow limits to corrected speed ratio can be expressed as a linear function of compressor pressure ratio. Specifically, it is assumed that

$$\frac{\dfrac{\dot{W}_T}{\delta\sqrt{\theta}}}{\dfrac{N}{\sqrt{\theta}}} = C_{10}\frac{P_3}{P_2} \qquad \text{(minimum flow)} \tag{C5}$$

$$\frac{\frac{\dot{W}_T}{\delta\sqrt{\theta}}}{\frac{N}{\sqrt{\theta}}} = C_{11}\frac{P_3}{P_2} + C_{12} \qquad \text{(maximum flow)} \qquad \text{(C6)}$$

Rewriting equations (C5) and (C6) yields

$$\dot{W}_{T(min)} = \frac{N}{P_r}(C_{10}P_3) \qquad \text{(C7)}$$

$$\dot{W}_{T(max)} = \frac{N}{P_r}\left[C_{10}P_3 + C_{12}P_2 + (C_{11} - C_{10})P_3\right] \qquad \text{(C8)}$$

A comparison between the fuel-control equations (C2) and (C4) and the engine fuel requirements (C7) and (C8) yields the following expressions from which the orifice areas A_{C1} and A_{C2} may be computed

$$A_{C1} = \frac{A_1}{P_r d}\left[C_{12}P_2 + (C_{11} - C_{10})P_3\right] \qquad \text{(C9)}$$

$$A_{C2} = \frac{A_1}{P_r d}C_{10}P_3 - A_1 \qquad \text{(C10)}$$

The coefficients C_{10}, C_{11}, and C_{12} must be evaluated from the minimum and maximum engine fuel requirements. For the J85-13 engine considered in the analysis of this report, these requirements were approximated by selecting

C_{10} = 1.54 (lbm/hr)/% speed	U.S. customary units
= 0.70 (kg/hr)/% speed	SI units
C_{11} = 4.15 (lbm/hr)/% speed	U.S. customary units
= 1.88 (kg/hr)/% speed	SI units
C_{12} = 8.195 (lbm/hr)/% speed	U.S. customary units
= 3.72 (kg/hr)/% speed	SI units

Substituting these values into the area relations of equations (C9) and (C10) and using values for d, P_r, V, and A_1 from table II results in

TABLE II. - CONSTANTS

Reference orifice area, A_1, $in.^2$; cm^2	3.24×10^{-3}; 20.9×10^{-3}
Maximum governor area, $\bar{A}_2$, $in.^2$; cm^2	0.15; 0.968
Governor piston area, A_p, $in.^2$; cm^2	1; 6.45
Conversion constants:	
C_1, $in.^2$; cm^2	2.2×10^{-3}; 14.2×10^{-3}
C_2, $in.^2/(lbf/in.^2)$; $cm^2/(N/cm^2)$	1.47×10^{-3}; 13.8×10^{-3}
C_3, $in.^2/(lbf/in.^2)$; $cm^2/(N/cm^2)$	3.55×10^{-4}; 33.2×10^{-4}
C_4, $in.^2$; cm^2	1.22×10^{-3}; 7.87×10^{-3}
C_5, $in.^2/(lbf/in.^2)$; $cm^2/(N/cm^2)$	2.10×10^{-4}; 19.7×10^{-4}
C_6, $in.^2/(lbf/in.^2)$; $cm^2/(N/cm^2)$	2.10×10^{-4}; 19.7×10^{-4}
C_{10}, (lbm/hr)/% speed; (kg/hr)/% speed	1.54; 0.70
C_{11}, (lbm/hr)/% speed; (kg/hr)/% speed	4.15; 1.88
C_{12}, (lbm/hr)/% speed; (kg/hr)/% speed	8.195; 3.72
Damping coefficient, D, (lbf)(sec)/in.; N-sec/cm	0.18; 0.315
Pump flow coefficient, d, (lbm/hr)/% speed; (kg/hr)/% speed	1.62; 0.737
Bias force, F_b, lbf; N	5; 22.24
Orifice flow conversion constant, k, $(lbm/hr)in.^2(lbf/in.^2)^{1/2}$; $(kg/hr)cm^2(N/cm^2)^{1/2}$	1.02×10^4; 863
Spring constant, k_1, lbf/in.; N/cm	75; 131.3
Spring constant, k_2, lbf/in.; N/cm	25; 43.8
Mass of governor spool, M, lbm; kg	0.327×10^{-3}; 0.0574
Reference pressure, P_r, $lbf/in.^2$; N/cm^2	14.7; 10.1
Maximum linear displacement of governor spool, $\bar{X}_s$, in.; cm	0.20; 0.508
Volume of chamber b, V_b, $in.^3$; cm^3	6; 98.32
Volume of chamber c, V_c, $in.^3$; cm^3	20; 327.7
Bulk modulus, β, $lbf/in.^2$; N/cm^2	1.5×10^5; 1.034×10^5
Fuel density, ρ, $lbm/in.^3$; kg/cm^3	0.0291; 0.806×10^{-3}

$$A_{C1} = 3.551\times10^{-4}\,(P_3 - P_2) + 14.7\times10^{-4}\,P_2 \qquad \text{U.S. customary units}$$

$$= 33.2\times10^{-4}\,(P_3 - P_2) + 138\times10^{-4}\,P_2 \qquad \text{SI units} \qquad \text{(C11)}$$

$$A_{C2} = 2.095\times10^{-4}\,(P_3 - P_2) + 2.095\times10^{-4}\,P_2 - 3.24\times10^{-3} \qquad \text{U.S. customary units}$$

$$= 19.7\times10^{-4}\,(P_3 - P_2) + 19.7\times10^{-4}\,P_2 - 20.9\times10^{-3} \qquad \text{SI units} \qquad \text{(C12)}$$

Equations (C11) and (C12) show that the equivalent areas A_{C1} and A_{C2} can be formed from the combination of an area proportional to compressor pressure rise and an area

proportional to compressor inlet pressure. These expressions can be used with equations (B23) and (B24) of appendix B to compute the following fuel control orifice areas:

$$A_{C1} = A_3 + A_4 \tag{C13}$$

where

$$A_3 = 3.55\times10^{-4}\,(P_3 - P_2) + a_{31} \quad \text{U.S. customary units}$$
$$= 33.2\times10^{-4}\,(P_3 - P_2) + a_{31} \quad \text{SI units}$$

$$A_4 = 14.7\times10^{-4}\,P_2 + a_{41} \quad \text{U.S. customary units}$$
$$= 138\times10^{-4}\,P_2 + a_{41} \quad \text{SI units}$$

$$A_{C2} = A_5 + A_6 \tag{C14}$$

where

$$A_6 = 2.095\times10^{-4}\,P_2 - 3.24\times10^{-3} \quad \text{U.S. customary units}$$
$$= 19.7\times10^{-4}\,P_2 - 20.9\times10^{-3} \quad \text{SI units}$$

$$A_5 = 2.095\times10^{-4}\,(P_3 - P_2) + a_{51} \quad \text{U.S. customary units}$$
$$= 19.7\times10^{-4}\,(P_3 - P_2) + a_{51} \quad \text{SI units}$$

In the simulation of the actual fuel control, the area expressions (C11) and (C12) were not exactly duplicated. The corresponding expressions for the design are:

$$\left.\begin{aligned} A_{C1} &= 3.55\times10^{-4}\,(P_3 - P_2) + 14.7\times10^{-4}\,P_2 - 22\times10^{-4} && \text{U.S. customary units} \\ &= 33.2\times10^{-4}\,(P_3 - P_2) + 138\times10^{-4}\,P_2 - 141.9\times10^{-4} && \text{SI units} \end{aligned}\right\} \tag{C15}$$

$$\left.\begin{aligned} A_{C2} &= 2.10\times10^{-4}\,(P_3 - P_2) + 2.10\times10^{-4}\,P_2 - 12.2\times10^{-4} && \text{U.S. customary units} \\ &= 19.7\times10^{-4}\,(P_3 - P_2) + 19.7\times10^{-4}\,P_2 - 78.7\times10^{-4} && \text{SI units} \end{aligned}\right\} \tag{C16}$$

Equations (C15) and (C16) are equivalent to the following engine minimum and maximum fuel-flow requirements:

For minimum flow

$$\left.\begin{aligned} \frac{\dot{W}_T}{\frac{\delta\sqrt{\theta}}{\frac{N}{\sqrt{\theta}}}} &= 1.544\,\frac{P_3}{P_2} + \frac{14.85}{P_2} && \text{U.S. customary units} \\ &= 0.7\,\frac{P_3}{P_2} + \frac{4.63}{P_2} && \text{SI units} \end{aligned}\right\} \qquad \text{(C17)}$$

For maximum flow

$$\left.\begin{aligned} \frac{\dot{W}_T}{\frac{\delta\sqrt{\theta}}{\frac{N}{\sqrt{\theta}}}} &= 4.153\,\frac{P_3}{P_2} + 8.195 - \frac{1.32}{P_2} && \text{U.S. customary units} \\ &= 1.88\,\frac{P_3}{P_2} + 3.72 - \frac{0.43}{P_2} && \text{SI units} \end{aligned}\right\} \qquad \text{(C18)}$$

It can be seen that equations (C15) and (C16) are close to equations (C11) and (C12). Equations (C17) and (C18) are close to equations (C5) and (C6) except that a term inversely proportional to inlet pressure P_2 is included. The effect of this term is illustrated by the scatter shown in figure 7. Since the purpose of the simulation was to demonstrate the feasibility of the design, the analytical work of this report is based on equations (C15) and (C16).

REFERENCES

1. Zalmanzon, L. A.; and Cherkasov, B. A.: Control of Gas-Turbine and Ramjet Engines. NASA TT F-41, 1961.

2. Sobey, Albert J.; and Suggs, Alfred M.: Control of Aircraft and Missile Powerplants. John Wiley & Sons, Inc., 1963.

3. Willoh, R. G.; and Seldner, K.: Multistage Compressor Simulation Applied to the Prediction of Axial Flow Instabilities. NASA TM X-1880, 1969.

4. Batterton, Peter G.; and Zeller, John R.: Dynamic Performance Analysis of a Fuel-Control Valve for Use in Airbreathing Engine Research. NASA TN D-5331, 1969.

NASA-Langley, 1970 —— 28 E-5263